TEMPERATURE DISTRIBUTION AND STRUCTURAL BEHAVIOR OF BOX-SECTIONAL ARCH STRUCTURES UNDER SOLAR RADIATION

Hongbo Liu [1], Zhihua Chen [1,2,*] and Ting Zhou [1]

[1] *Department of Civil Engineering, Tianjin University, Tianjin 300072, China*
[2] *Tianjin Key Laboratory of Civil Engineering Structure & New Materials, Tianjin University, Tianjin 300072, China*
**(Corresponding author: E-mail: zhchen@tju.edu.cn)*

Received: 24 March 2012; Revised: 25 May 2012; Accepted: 31 May 2012

ABSTRACT: The temperature change of large-span steel arch structures normally appears when the structures are exposed to solar radiation, which may result in large displacement and stress. Therefore, there has been growing attention to both temperature distribution and structural response of the structures under the solar radiation. In order to investigate the response of large-span box-sectional steel arch structures formed by rectangular steel tubes, one rectangular steel tube specimen was designed and its temperature was measured under solar radiation. A numerical method was presented according to transient thermal analysis and then verified by experimental results. Both experimental and numerical results showed that the solar radiation had a significant effect on the temperature distribution of rectangular steel tubes. Considering the solar radiation, the temperature of rectangular steel tubes is about 18.1^{o}C higher than the corresponding ambient air temperature in summer. Moreover, the temperature distribution under solar radiation is extremely nonlinear. In order to study the structural response induced by the temperature change due to the solar radiation, a steel arch structure model is designed and the structural response due to temperature change is also investigated on this model. The results showed that the solar radiation has a remarkable effect on the thermal load response of large-span steel structures. The effect of the solar radiation has to be considered in the design process of large-span steel arch structures.

Keywords: Effective box-sectional steel arch structures, Temperature change, Solar radiation, Rectangular steel tube, Numerical analysis, Structural response

1. INTRODUCTION

In recent years, large-span steel structures, such as arch structures, beam string structures, suspen-dome structures, lattice shell structures and cable-strut structures, are widely adopted as the roof structures of stadiums, gymnasiums, conference, exhibition center, train stations, airport and so on. Most constructed steel structures have a span more than 200 m. For example, the arch structures of the Baita Airport, Inner Mongolia, China is 205 m as shown in Figure 1. Due to the large span, the steel structure is sensitive to the thermal change, especially when exposed to solar radiation. Therefore, the thermal load is usually the control load for large-span steel structures and there has been growing attention to the structural behavior of steel structures under thermal change.

Figure 1. Baita Airport, Inner Mongolia, China

Alinia and Kashizadeh conducted some work on the structural behavior of spherical double layer space truss domes under uniform thermal load [1-3]. However, for the steel structures exposed to solar radiation, its temperature is much larger and more non-uniformly distributed than the corresponding ambient air temperature in summer. If the effect of solar radiation on the temperature of steel structures is not considered properly, the steel structure may potentially fail due to over-large temperature change. However, only a few published papers were reported on the temperature distribution of steel structures under solar radiation. In addition, a number of researchers drew inconsistent conclusions on this problem. For example, three maximal temperatures under solar radiation for steel structures proposed by Fan et al. [4], Wang et al. [5] and Xiao et al. [6] are 50℃, 60℃ and 80℃, respectively. Therefore, this inconsistency may make the one confused to determine the thermal effect in the design process.

The available references, on the thermal effect due to the solar radiation, have focused on bridges [7-8], dams [9-10] and pavements [11-12]. Considering the large structural difference among large-span steel structures, bridges, dams and pavements, the proposed numerical methods in these papers are not directly applied to large-span steel structures. Therefore, it is important to understand the temperature distribution of large-span steel structures under solar radiation through both experimental and numerical studies.

In this study, an experiment first was conducted to provide insights into the temperature distribution of steel members under solar radiation in summer, as well as to verify a following numerical simulation method. And then the numerical simulation method is presented for the temperature distribution analysis of steel members under solar radiation. This method is further verified by the test data. Using the numerical simulation method, the temperature distribution of an arch structure under solar radiation in summer is analyzed. Meanwhile, the structural behavior under thermal effect is also studied to give the temperature-induced response of large-span steel arch structures.

2. EXPERIMENTAL STUDY

2.1 Experiment Program

A rectangular steel tube specimen was designed and measured to obtain its temperature distribution under solar radiation as shown in Figure 2. Figure 3 presents twelve measured points designed for this specimen. In this test, infra-red temperature meter was used to obtain the temperature value of each measured point.

Figure 2. Specimen in Test Site

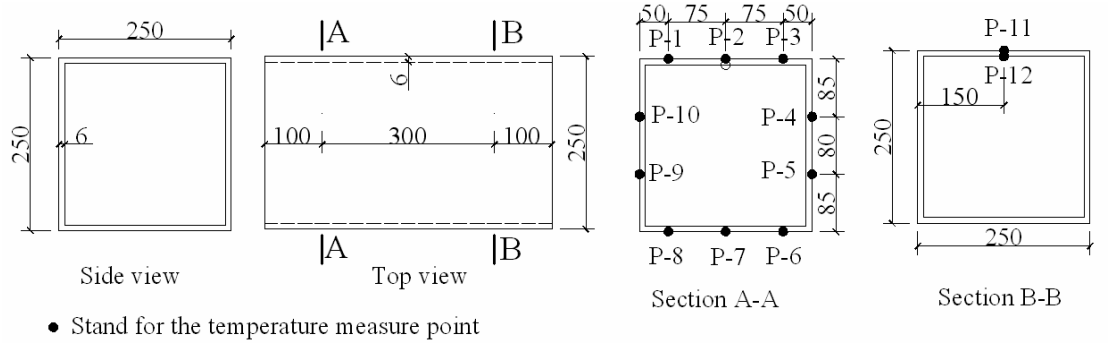

Figure 3. Arrangement of Temperature Measure Points of the Rectangular Steel Tube Specimen

2.2 Experiment Result

For the rectangular steel tube specimen, the temperature values of all measure points arranged in Figure 3 were obtained at 6:00 am, 8:00 am, 10:00 am, 12:00 am, 13:00 pm, 14:00 pm, 15:00 pm, 16:00 pm, 17:00 pm, 18:00 pm and 19:00 pm on 22th, 23th and 24th July, 2010.

The temperature-time curve for the maximal temperature point (Point 2) and the minimal temperature point (Point 7) are shown in Figure 4 and Figure 5. The temperature values for all measure points at 14 pm are given in Figure 6 and Figure 7. The following conclusions can be drawn on the test results:

1) The temperature-time curve for Point 2 and Point 7 is similar to sine curve as shown in Figure 4 and Figure 5.

2) The maximal temperature value obtained in this experiment is $52.3\,^{0}C$, $18.1\,^{0}C$ higher than the corresponding ambient air temperature with a value of $34.2\,^{0}C$; and the maximal temperatures usually occur at 12:00~14:00 as shown in Figure 4, Figure 5 and Table 1.

3) The temperature of the specimen begins to increase and then decrease from Point 1 to Point 10 at 14:00 pm as shown in Figure 6. Therefore, the temperature distribution is non-uniform on the whole specimen. However, for the upper steel plate and low steel plate in the rectangular steel tube specimen, their temperature distribution is almost uniform.

4) The temperature-time curve of Point 11 is identical to that of Point 12 as shown in Figure 7. Therefore, the temperature distribution in thickness direction is uniform.

5) The temperature-time curve of Point 2 is identical to that of Point 11 as shown in Figure 7. Therefore, the temperature in the longitudinal direction is uniform if the two ends of rectangular steel tubes are close to each other.

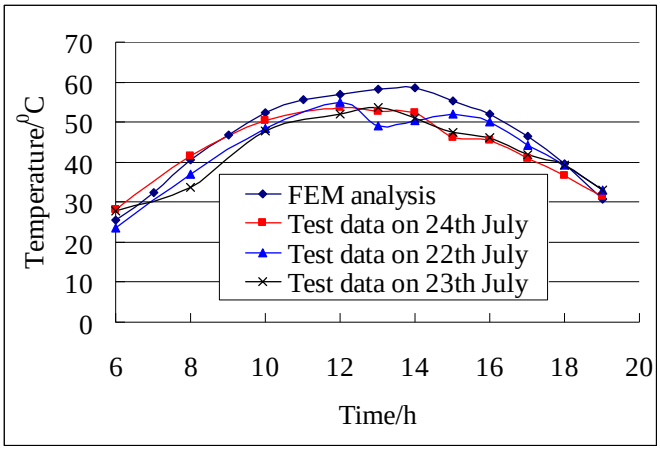

Figure 4. Time-temperature Curve of Point 2

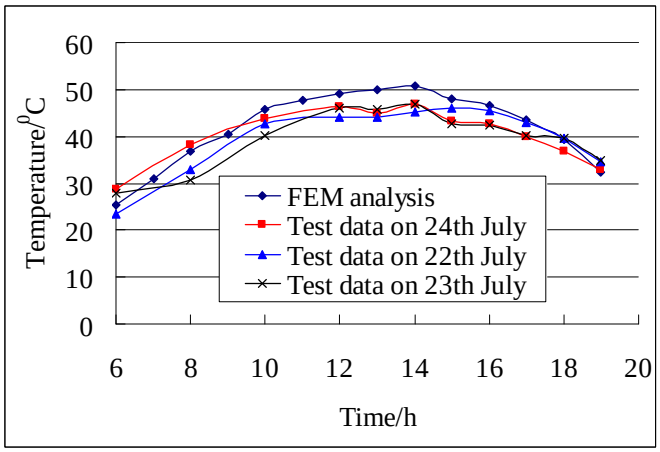

Figure 5. Time-temperature Curve of Point 7

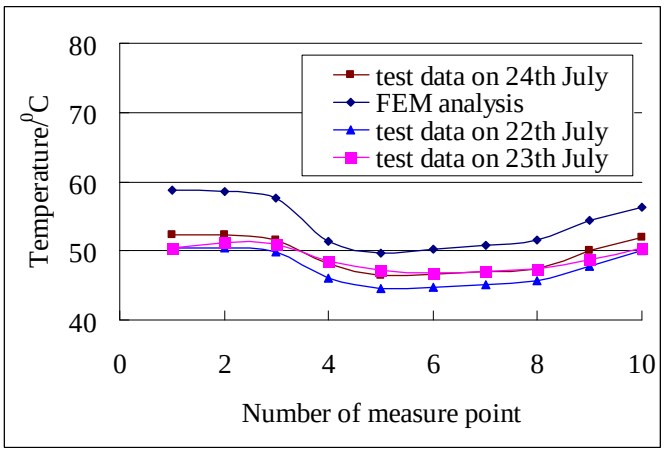

Figure 6. Temperature of All Points at 14:00 pm

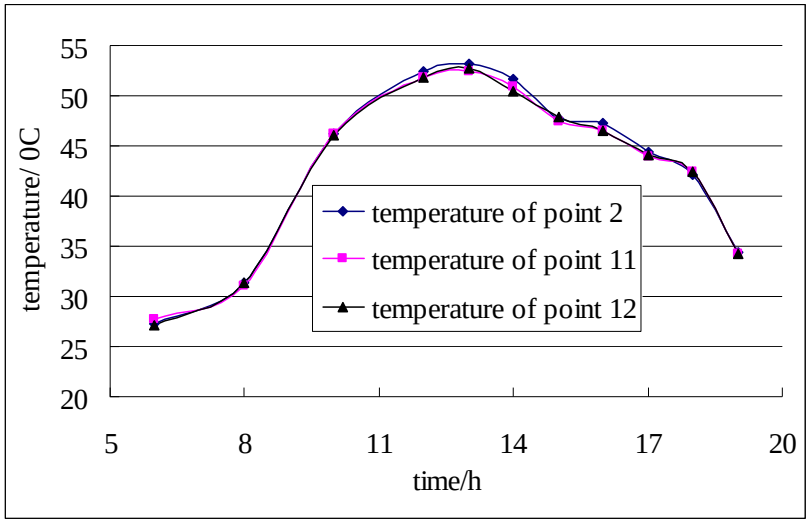

Figure 7. Time-temperature Curves of Point 1 and Point 10 on 22th July, 2010

Table 1. Minimal and Maximal Temperature Values of the Rectangular Steel Tube Specimen at 14:00

Item	T_{test22}	T_{test23}	T_{test24}	T_{FEM}	error-max
Min temperature	44.7	46.9	46.4	48.98	8.74%
Max temperature	50.4	51.1	52.3	59.07	14.68%

3. NUMERICAL SIMULATION

3.1 Heat Conduction Equation

According to previous references, the thermal properties of steel material are assumed to be uniform and isotropic. Considering that there is no heat generation within rectangular steel tubes, the general transient governing equation for heat conduction in a three dimensional solid region Ω can be expressed as follows:

$$\alpha\left(\frac{\partial^2 T}{\partial x^2}+\frac{\partial^2 T}{\partial y^2}+\frac{\partial^2 T}{\partial z^2}\right)=\frac{\partial T}{\partial t} \tag{1}$$

where $\alpha=\lambda/\rho c$; λ is thermal conductivity($w/m^{2\,0}C$); ρ is material's density (kg/m^3); c is specific heat ($J/kg^{0}C$).

3.2 Boundary Conditions

In the process of thermal analysis using a three-dimensional finite element, the temperature boundary conditions should be first determined. For the rectangular steel tubes, the temperature is affected by solar radiation, convection heat transfer and long wave radiation heat transfer. Therefore, the temperature boundary condition is defined as:

$$\lambda\left.\frac{\partial T}{\partial n}\right|_{\Gamma}=h\left[T_a(t)-T\right]+q_S(t)+q_L(t) \tag{2}$$

Where h is heat convection coefficient ($w/m^{2\,0}C$); T_a is ambient air temperature; q_s is solar radiation (w/m^2); q_l is long wave radiation (w/m^2).

3.3 Solar Radiation Model

The ASHRAE clear-sky model was adopted in this study to evaluate the solar radiation on the surface of rectangular steel tubes [13]. In this model, the total global solar radiation is assumed to be the sum of direct radiation, diffuse radiation, and the solar radiation reflected from the surrounding surface. On a clear day, the value of solar radiation at the earth's surface is defined as

$$G_{ND} = \frac{A}{\exp(B/\sin\beta)} C_N \tag{3}$$

Where: G_{ND} = normal direct radiation, W/m^2; A = apparent solar radiation at air mass equal to zero, W/m^2; B = atmospheric extinction coefficient; β = solar altitude; C_N = clearness number
Based on the ASHRAE model, the total solar radiation incident on a non-vertical surface can be evaluated by Eq. 4 :

$$q_s = \varepsilon\left[\max(\cos\theta, 0) + CF_{ws} + \rho_g F_{wg}(\sin\beta + C)\right] G_{ND} \tag{4}$$

$$F_{ws} = (1+\cos\alpha)/2 \tag{5}$$

$$F_{wg} = (1-\cos\alpha)/2 \tag{6}$$

Where ε is the solar radiation absorptivity; θ is the angle of incidence between the sun's rays and the normal to the surface; α is tilt angle; C is obviously the ratio of diffuse irradiation on a surface to direct normal radiation; F_{ws} the angle factor between the surface and the sky; F_{wg} is the configuration or angle factor from surface wall to ground; ρ_g is the solar radiation reflectance of ground or horizontal surface

Similarly, the total solar radiation incident on a vertical surface can be given by following equations:

$$q_s = \varepsilon\left[\max(\cos\theta, 0) + \frac{GdV}{G_{dH}} C + \rho_g F_{wg}(\sin\beta + C)\right] G_{ND} \tag{7}$$

$$\frac{G_{dV}}{G_{dH}} = \begin{cases} 0.55 + 0.437\cos\theta + 0.313\cos^2\theta & \theta > -0.2 \\ 0.45 & \text{otherwise} \end{cases} \tag{8}$$

The parameters A, B, and C can be determined according to the characteristics of solar radiation at the experiment site. Unfortunately, this information is not yet available. To overcome this problem, the following expressions of parameters A, B, and C for Beijing, near to test site, were adopted to evaluate solar radiation [14].

3.4 Long Wave Radiation

The long wave radiation on the surface of rectangular steel tubes can be expressed by the Stefan-Boltzmann equation [13]:

$$q_l = \varepsilon_f \sigma (F_{wg}(T_g^4 - T^4) + F_{ws}(T_{sky}^4 - T^4)) \tag{9}$$

Where ε_f is the ratio of the radiation emitted by a surface; σ is Stefan-Boltzmann constant= $5.67\times10^{-8} W/(m^2 \cdot K^4)$; T_{sky} is the effective temperature of sky, usually calculated by $T_a - 6$; T_g is the ground temperature.

3.5 Numerical Investigation

A finite element model is established using ANSYS software, and a three-dimensional thermal conduction element SOLID70 is used to simulate the rectangular steel tube specimen. The physical properties of steel material and the main parameters used in the study are listed in Table 2.

Table 2. Parameters Adopted in Calculation

Parameters	Convection coefficient $W/(m^2 \cdot {}^0C)$	Specific heat capacity $J/(kg \cdot {}^0C)$	Thermal conductivity $W/(m \cdot {}^0C)$
Values	13.3	480	56
Parameters	Absorptivity	Density (kg/m^3)	Emissivity
Values	0.6	7850	0.8
Parameters	Coefficient A	Coefficient B	Coefficient C
Values	1326.54	0.404	0.181
Parameters	Ground radiation reflectance ρ_g	c_N	
Values	0.15	1.0	

The temperature obtained from the transient thermal analysis of the specimen was also shown in Figure 4 through Figure 7 and Table 1. T_{FEL} (obtained from the finite element analysis) was generally larger than T_T (obtained from test) by a factor of 1.0 to 1.5. Therefore, the strength TFEL was generally consistent with the test results, with a maximum difference of 14.68%.

Reasons attributing to the discrepancies may include variance in the solar radiation model, variance in solar radiation absorption and ground reflectance, precision of infra-red temperature meter, etc. In the test process, the clouds might shelter against solar radiation, and it decreased the temperature of the rectangular steel tube specimen. Considering the above arguments, the numerical results for the rectangular steel tube specimen were then considered generally precise, and the transient models can be used for the following parametric study.

The temperature distribution of the rectangular steel tube specimen at 14:00 on 22th July 2010 is shown in Figure 8(a). From this figure, the temperature field under solar radiation is found to be very non-uniform. However, because the two ends of rectangular steel tubes are close to each other in practice, the temperature field of the specimen is analyzed under the condition that the solar radiation cannot irradiate the inner surface of specimen. The corresponding temperature field is shown in Figure 8(b). The numerical results showed the temperature is longitudinally uniform if the two ends of rectangular steel tube is close to each other.

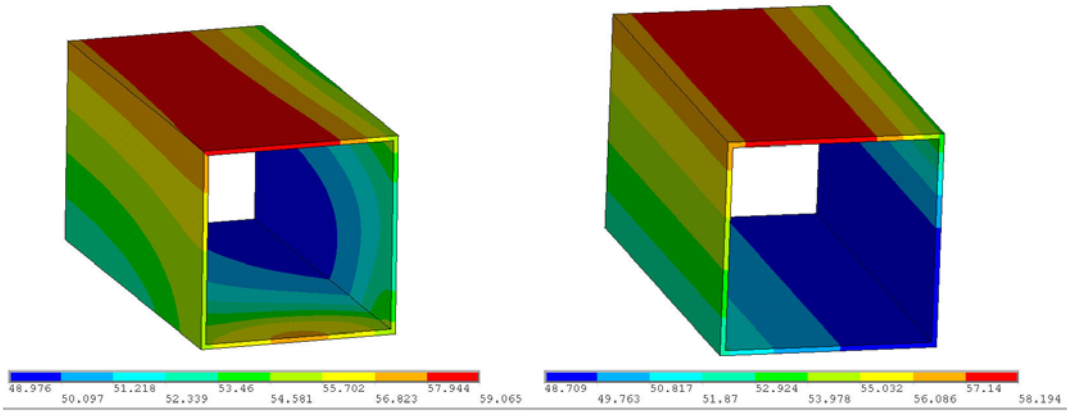

(a) Consider solar radiation shadow (b) Not consider solar radiation shadow

Figure 8. Temperature Distribution of the Rectangular Steel Tube Specimen at 14:00 pm on 22th July 2010

4. APPLICATION

4.1 A Steel Arch Structure Model

In order to understand the temperature distribution and thermal behavior of large-span arch structures, a steel arch structure was designed as shown in Figure 10. Its span and rise is 200 m and 40 m, respectively. The tapered rectangular steel tubes were used as the members. For the tapered rectangular steel tube, its flange width is constant with a value of 1.4 m, and its web height ranges from 1.4 m at the mid-span to 1.8 m at both ends.

The model consists of 89 structural members with rectangular sections. Each structural member includes four areas. Therefore, 356 areas are included in this model. The area number of Area A is 1 ~ 89 from End J to End I. The area number of Area B is 90 ~ 178 from End J to End I. The area number of Area C is 179 ~ 267 from End J to End I. The area number of Area D is 268 ~ 356 from End J to End I.

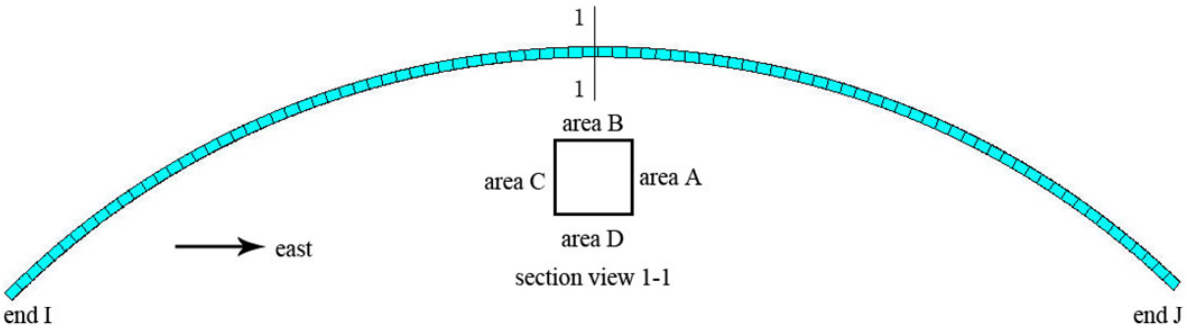

Figure 10. The Model of the Arch Structure in ANSYS

4.2 Temperature Distribution Simulation

Using the numerical simulation method presented in this paper, the temperature distribution of the steel arch structure model on 21th June was analyzed. The temperature distribution of the model at 14:00 p.m. is shown in Figure 11. The average temperatures for all areas at 6:00 a.m., 14:00 p.m. and 19:00 p.m. are shown in Figure 12. From the figures, the following conclusions are obtained:

1) The maximal temperature for the studied model occurred at 14:00 p.m. and the value is 65.28℃.

2) The temperature distribution is very no-uniform and the temperature variance is up to 20℃. At 14:00 p.m., the average temperature of Area B is the largest; the average temperature of Area D is the smallest.

3) The temperature change is large from sunrise to sundown. It is up to 40℃ during a day

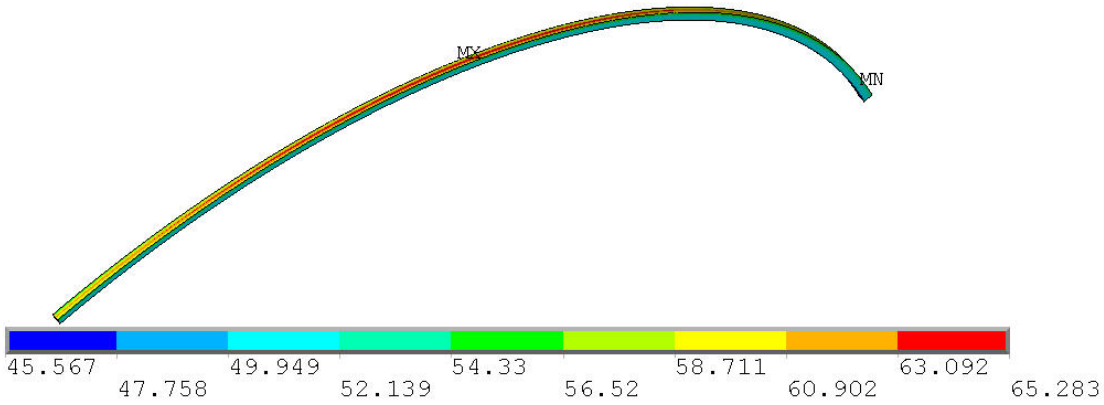

Figure 11. The Temperature Distribution of the Studied Model at 14:00 p.m.

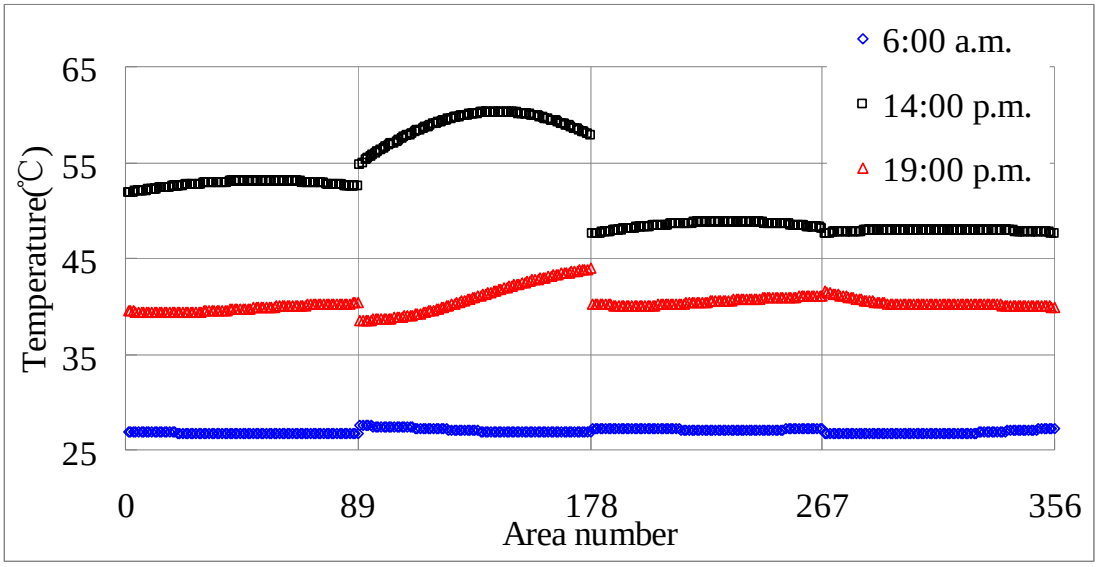

Figure 12. The Average Temperatures for All Areas at 6:00 a.m., 14:00 p.m. and 19:00 p.m.

4.3 Thermal Behavior

Assume that the highest and the lowest air temperature for the steel arch structure model location is 40℃ and -20℃, respectively. If the effect of solar radiation is not considered, the healing temperature should be 10℃. In order to investigate the effect of solar radiation on the thermal–induced response of the model, two cases are designed. The solar radiation is not considered in the first case, and this case denote as Case A. The positive thermal value in Case A is uniform and the value is 30℃. The solar radiation is considered in the other case, and this case denote as Case B. The positive thermal value in Case B is no-uniform load and the value fluctuates from 35.57℃ to 55.28℃.

The support conditions at the two ends are assumed to be pinned. Compared with the maximum equivalent stress of 84.2 MPa and the maximum node displacement of 99 mm of Case A, the corresponding values of Case B are 150.6 MPa (78.86% increased) and 165 mm (66.67% increased), respectively. Therefore, the solar radiation has a remarkable effect on the thermal-induced response of large span steel structures.

5. CONCLUSIONS

1) From the test result, the following conclusions are drawn: i) the temperature-time curve is similar to a sine curve; ii) the temperature obtained in this experiment is $52.3\,^{0}C$, it is $18.1\,^{0}C$ higher than the corresponding ambient air temperature; iii) the maximal temperatures usually occur during 12:00~14:00 ; iv) the temperature field is very non-uniform under solar radiation.

2) The presented numerical simulation method on the temperature distribution of steel members under solar radiation is verified by the test data.

3) The solar radiation has a remarkable effect on the temperature-induced response of large-span steel structures.

ACKNOWLEDGEMENTS

This work was supported by the National Natural Science Foundation of China (No. 51208355), China Postdoctoral Science Foundation funded project (No. 2012M510751) and the Independent innovation foundation of Tianjin University (No. 1102, No. 1104).

REFERENCES

[1] Alinia, M.M., Kashizadeh, S., “Effect of Flexibility of Substructures Upon Thermal Behaviour of Spherical Double Layer Space Truss Domes, Part I : Uniform Thermal Loading”, Journal of Constructional Steel Research, 2006, Vol. 62, pp. 359-368.

[2] Alinia, M.M., Kashizadeh, S., “Effect of Flexibility of Substructures upon Thermal Behaviour of Spherical Double Layer Space Truss Domes, Part II : Gradient & Partial Loading”, Journal of Constructional Steel Research, 2006, Vol. 62, pp. 675-681.

[3] Alinia, M.M., Kashizadeh, S., “Effects of Support Positioning on the Thermal Behaviour of Double Layer Space Truss Domes”, Journal of Constructional Steel Research, 2007, Vol. 63, pp. 375-382.

[4] Fan, Z., Wang, Z. and Tian, J., ”Analysis on Temperature Field and Determination of Temperature upon Healing of Large-span Steel Structure of the National Stadium”, Journal of Building Structures, 2007, Vol. 28, No. 2, pp. 32-40. (in Chinese)

[5] Wang, Y.Q., Lin, C.C. and Shi, Y.J., “Experimental Study on the Temperature of Steel Members in Sunshine”, Journal of Building Structures, 2010, Supplementary Issue 1, pp. 140-147. (in Chinese)

[6] Xiao, J.C., Xu, H., Liu, J.K. and Ma, K.J., “The Influence of Intense Solar Radiation on Long-span Spatial Steel Structures”, Chinese Journal of Solid Mechanics, 2010, Vol. 31 (Issue), pp. 275-280. (in Chinese)

[7] Xu, Y.L., Chen, B., Ng, C.L., Wong, K.Y. and Chan, W.Y., “Monitoring Temperature Effect on a Long Suspension Bridge”, Structural Control and Health Monitoring, 2010, Vol. 17, pp. 632–653.[8] Tong, M., Tham, L.G. and Au, F.T.K., “Numerical Modeling for Temperature

Distribution in Steel Bridges", Computers and Structures, 2000, Vol. 79. pp. 583-593.
[9] Jin, F., Chen, Z., Wang, J.T. and Yang, J., "Practical Procedure for Predicting Non-uniform Temperature on the Exposed Face of Arch Dams", Applied Thermal Engineering, 2010, Vol. 20, pp. 2146-2156.
[10] Noorzaei, J., Bayagoob, K.H., Thanoon, W.A., et al., "Thermal and Stress Analysis of Kinta RCC Dam", Engineering Structures, 2006, Vol. 28, No. 13, pp. 1795-802.
[11] Brisn, K. Diefenderfer, Imad, L. Al-Qadi, Stacey, D. Diefenderfer, "Model to Predict Pavement Temperature Profile : Development and Validation", Journal of Transportation Engineering, Vol. 132, No. 2, pp. 162-167.
[12] Chiasson, Andrew D., Yavuzturk, Cenk, Ksaibati, Khaled, "Linearized Approach for Predicting Thermal Stresses in Asphalt Pavements due to Environmental Conditions", Journal of Materials in Civil Engineering, Vol. 20, No. 2, pp. 118-127.
[13] McQuiston, Faye C., Parker, Jerald D., Spitler, Jeffrey D., "Heating, Ventilating, and Air Conditioning Analysis and Design", USA : John Wiley and Sons, 2005.
[14] Li, J.P. and Song, A.G., "Compare of Clear Day Solar Radiation Model of Beijing and ASHRAE", Journal of Capital Normal University, 1998, Vol. 19, No. 1, pp. 35-38.(in Chinese).